Journal of Biomedical Optics

BiomedicalOptics.SPIEDigitalLibrary.org

Photodynamic therapy with chlorin-based photosensitizer at 405 nm: numerical, morphological, and clinical study

Maria Shakhova
Daria Loginova
Alina Meller
Dmitry Sapunov
Natalia Orlinskaya
Andrey Shakhov
Alexander Khilov
Mikhail Kirillin

SPIE.

Maria Shakhova, Daria Loginova, Alina Meller, Dmitry Sapunov, Natalia Orlinskaya, Andrey Shakhov, Alexander Khilov, Mikhail Kirillin, "Photodynamic therapy with chlorin-based photosensitizer at 405 nm: numerical, morphological, and clinical study," *J. Biomed. Opt.* **23**(9), 091412 (2018), doi: 10.1117/1.JBO.23.9.091412.

Photodynamic therapy with chlorin-based photosensitizer at 405 nm: numerical, morphological, and clinical study

Maria Shakhova,[a,b,*] Daria Loginova,[a,c] Alina Meller,[a,b] Dmitry Sapunov,[a,b] Natalia Orlinskaya,[a,b] Andrey Shakhov,[a,b] Alexander Khilov,[a] and Mikhail Kirillin[a]
[a]Institute of Applied Physics RAS, Nizhny Novgorod, Russia
[b]Nizhny Novgorod State Medical Academy, Nizhny Novgorod, Russia
[c]N.I. Lobachevsky State University of Nizhny Novgorod, Advanced School of General and Applied Physics, Nizhny Novgorod, Russia

Abstract. Employment of chlorin-based photosensitizers (PSs) provides additional advantages to photodynamic therapy (PDT) due to absorption peak around 405 nm allowing for superficial impact and efficient antimicrobial therapy. We report on the morphological and clinical study of the efficiency of PDT at 405 nm employing chlorin-based PS. Numerical studies demonstrated difference in the distribution of absorbed dose at 405 nm in comparison with traditionally employed wavelength of 660 nm and difference in the in-depth absorbed dose distribution for skin and mucous tissues. Morphological study was performed at the inner surface of rabbit ear with histological examinations at different periods after PDT procedure. Animal study revealed tissue reaction to PDT consisting in edema manifested most in 3 days after the procedure and neoangiogenesis. OCT diagnostics was confirmed by histological examination. Clinical study included antimicrobial PDT of pharynx chronic inflammatory diseases. It revealed no side effects or complications of the PDT procedure. Pharyngoscopy indicated reduction of inflammatory manifestations, and, in particular cases, hypervascularization was observed. Morphological changes were also detected in the course of monitoring, which are in agreement with pharyngoscopy results. Microbiologic study after PDT revealed no pathogenic bacteria; however, in particular cases, saprophytic flora was detected. [DOI: 10.1117/1.JBO.23.9.091412]

Keywords: photodynamic therapy; optical coherence tomography; chlorin-based photosensitizers; Monte Carlo simulations.

Paper 180075SSRR received Feb. 2, 2018; accepted for publication May 31, 2018; published online Jun. 28, 2018.

1 Introduction

Photodynamic therapy (PDT) is a modern minimally invasive treatment technique that has demonstrated efficiency for a wide range of clinical applications. Currently, PDT is actively employed for antitumor treatment[1,2] and is being involved in antimicrobial and anti-inflammatory action due to high resistance of these pathologies to drug treatment.[3–8] Recently, PDT was introduced as a technique for skin antiaging treatment in aesthetic medicine.[9–14] PDT is a multifactor approach involving three main components, namely, photosensitizer (PS), light, and oxygen. The main PDT effects induced by the photodynamic reactions are direct cytotoxic impact to cells, tumor vasculature damage, and immune reactions.[1,2,15,16] Along with high efficiency the advantages of PDT include minimal invasiveness to surrounding healthy tissues and weak systemic effects that ensure organ preservation and good functional results.

Reported PDT studies prove its efficiency and allow one to predict its wider employment in clinical practice indicating, however, the possibility and the need for the technique optimization.[4,15–17] One of the ways for PDT advancement is the optimization of the PDT regimes.

PDT procedure can be enhanced by employment of additional illumination wavelength for alternative or complementary light exposure.[17–22] Chlorin-type PSs have two pronounced absorption peaks in the red and blue regions of the visible range. Traditionally, red light is employed for PDT owing to its deeper penetration into tissues as compared with blue one. However, complementary application of both wavelengths could be advantageous given better knowledge on fluence distribution with particular treated tissues and tissue reactions to the procedure.

Currently, there is no unified opinion on the results of the application of these optical ranges. On the one hand, it was demonstrated that employment of the optical range of 400 to 450 nm provides higher safety in case of vast pathologic areas;[18] paper[20] demonstrates higher efficacy of blue light in antiaging skin impact, whereas other groups report that no significant differences in applications of different optical ranges were revealed.[21] It is worth mentioning that the effects of different optical ranges in PDT are studied insufficiently both from the point of view of antibacterial effects and morphological and pathophysiological reactions of tissues. Comparison of application of different light sources for inactivation of various organisms in anti-inflammatory PDT is reported in paper,[6] whereas paper[22] is one of the few reporting an attempt to analyze PDT mechanisms and reactions depending on the wavelengths employed.

Another way of optimization of a PDT procedure and its efficiency increase consists in account for individual patient

*Address all correspondence to: Maria Shakhova, E-mail: maha-shakh@yandex.ru

1083-3668/2018/$25.00 © 2018 SPIE

features and corresponding correction of impact regimens. Monitoring of PDT procedure allows for real-time evaluation of tissue reaction via parameters related to PS accumulation and photobleaching and, if necessary, correction of the PDT course. Imaging techniques are of key importance for tissue monitoring in the course of PDT procedure. Optical imaging techniques have high potential in this application due to the ability for real-time noninvasive monitoring of the efficiency of photodynamic reaction in combination with compactness and economic efficacy.[23–25] Most of the studies employ fluorescence imaging (FI) allowing one to evaluate PS accumulation level, monitor PS photobleaching, and clarify the tumor border in oncologic applications.[26–30] Combination of FI with spectroscopy techniques allows for simultaneous monitoring of singlet oxygen production in the course of PDT procedure.[31,32] Optical coherence tomography (OCT) allows for assessment of immediate tissue morphologic response and PDT procedure outcomes.[33,34] Recently, OCT angiography was reported to provide monitoring of functional tissue response to PDT.[35] Evaluation of the post PDT microvascular damage from OCT angiography may serve as an indicator of the PDT efficiency. Multimodal approaches with hybrid or complementary use of optical imaging techniques were reported in several studies.[36–38] An important aspect consists in further improvement of the abilities of optical imaging techniques for monitoring of microcirculation in the course of PDT.[39,40]

This paper combines three aspects of employing PDT with chlorin-based PS with irradiation at the wavelength of 405 nm compared with traditionally employed wavelength of 660 nm: numerical simulation of light propagation allows one to evaluate the distribution of the absorbed dose in tissue, animal study reveals differences in tissue response to PDT, whereas clinical studies report on treatment results for PDT with optical monitoring assistance.

Numerical studies include comparison of spatial distribution of the absorbed dose within tissue for the wavelengths of 405 and 660 nm derived from the results of Monte Carlo simulations. Animal study includes monitoring of PDT procedures at two specified wavelengths by complementary use of OCT and FI with subsequent histological studies. Pilot human studies demonstrate the efficiency of antimicrobial PDT for treatment of inflammatory pathologies of pharynx assisted by visual and OCT monitoring.

2 Materials and Methods

2.1 *Monte Carlo Simulations*

In this study, we employed previously developed Monte Carlo code[41,42] to simulate dose absorption maps for irradiation of skin and mucous tissue at the wavelengths of 405 and 660 nm and compare typical impact depths. Monte Carlo technique is based on the simulation of a large number of random photon walks in a given turbid medium with the specified optical properties and subsequent statistical analysis of the collected data.

The simulation was performed for uniform illumination with a total light dose of 50 J/cm^2 (0.5 J/mm^2) at the surface that corresponded to the parameters of the regimes employed in animal and clinical studies. When describing the simulation results all the delivered doses are given in J/mm^2 and absorbed dose densities are given in J/mm^3 because the typical scale is of order of mm.

Table 1 Typical optical properties of skin and mucous tissues at the wavelengths of 405 and 660 nm.[43–46]

			405 nm		660 nm	
	d (mm)	g	μ_a (mm^{-1})	μ_s (mm^{-1})	μ_a (mm^{-1})	μ_s (mm^{-1})
Skin						
Stratum corneum	0.05	0.9	20	200	10	200
Epidermis	0.15	0.8	1.3	35	0.3	23
Dermis	3.8	0.8	0.9	27	0.15	14
Mucosa	4	0.8	0.5	18	0.01	6

We considered a three-layer skin model, consisting of stratum corneum (50 μm), epidermis (150 μm), and dermis (3.8 mm), and a single layer model for mucous tissues. Tissue optical properties employed in Monte Carlo simulations are summarized in Table 1. The refractive index amounted 1.4 for all the layers.

2.2 *Animal Study*

Morphological and functional changes in tissues as a result of PDT procedure were studied at the skin of a rabbit ear inner surface. The studies are approved by the Ethical Committee of the Nizhny Novgorod State Medical Academy (Protocol #13, 03.10.2017). Topically applied drug "Revixan" (Revixan Ltd., Russia) based on chlorin-type PS was employed in the study. The drug contains pure chlorin e6 in a concentration of 0.1% vol. The "Revixan" gel in the amount of 2 mL was administered to the rabbit ear inner surface with a cotton swab. In 20 min after application the rest of the gel was removed, as well, with a cotton swab. A laser at the wavelength of 405 nm (M-33A405-500-G, Shenzhen 91 Laser Co., Ltd., China) was employed as a light source; the total impact light dose was 50 J/cm^2. The dose was chosen in accordance with the typical doses employed in antimicrobial PDT (for example, see Refs. 47–49). The irradiance at the tissue area was tuned to 0.4 W/cm^2 resulting in total illumination time of 125 s. The treated area was 2×3 cm^2, a total of six areas were treated. Optical monitoring of a PDT procedure was performed by OCT (OCT-1300E device, BioMedTech, IAP RAS, Nizhny Novgorod, Russia) and FI (fluorescence imaging device,[50] IAP RAS, Nizhny Novgorod, Russia). OCT imaging was performed before PS administration (intact tissue), in 15 min after PS administration, immediately after laser impact, in 1, 3, and 7 days after PDT procedure.

The tissue changes were verified morphologically. Biopsy samples for histological studies were taken in 1, 3, and 7 days after the PDT procedure. Biopsy samples were subjected to staining with hematoxylin-eosin. Morphological studies were performed employing Leica DM 2500 microscope. The following parameters were analyzed: signs of edema and inflammation and the area of the newly formed vessel. The degree of edema (percentage of edema lumen between tissue elements) and inflammation (the presence of neutrophils and lymphocytes) was evaluated by semiquantitative three-grade scale depending on the manifestation in histology images (criteria are shown in

Table 2 Semiquantitative scale for evaluation of the degree of edema and inflammation.

Score	Manifestation degree	Criteria for edema	Criteria for inflammation
+	Weak	edema lumen percentage <15%	1 to 5 neutrophils in the field of view
++	Moderate	edema lumen percentage between 15% and 25%	5 to 10 neutrophils in the field of view, presence of plethora
+++	Pronounced	edema lumen percentage between >25%	>10 neutrophils in the field of view, presence of plethora

Table 2). Criteria for moderate and pronounced inflammation also include the presence of plethora, which is manifested by the excessive presence of erythrocytes in the dilated vessel lumens. For each score, an average over 10 fields of view was taken; a field of view size is 0.65×0.44 mm (×400 magnification).

The area of the newly formed vessels lumen was calculated as the relative area of newly formed vessels lumens in histology images averaged over 10 fields of view. The newly formed vessels were distinguished in the histology images as small vessels with thin walls and young endotheliocytes. The variation of the area was expressed in percentage with respect to the control value before PDT procedure.

2.3 *Human Subject Study*

Evaluation of the efficiency of antimicrobial PDT was performed in the frames of a clinical study. The study was approved by the Ethical Committee of Nizhny Novgorod State Medical Academy (Protocol #7, 03.07.2017) for studies with human subjects. All the patients signed an informed written consent. A total of eight patients with exacerbation of chronic pharyngitis were enrolled in the study and underwent antibacterial PDT treatment. For all the patients, a microbiology study was performed to determine the etiology of the diseases and OCT inspection of pharynx mucosa was made to evaluate its morphological and functional condition. Each patient underwent three PDT procedures performed daily (days 1, 2, and 3; day 1 is the day of the first PDT procedure); visual and OCT inspection of the treated area was performed after each procedure and then in 3 and 7 days after the first procedure (days 1, 2, 3, 4, and 8). PDT procedure was performed in the course of standard pharyngoscopy inspection with topically applied chlorin-based drug "Revixan" (Revixan Ltd., Russia) in the form of gel. The drug contains pure chlorin e6 in a concentration of 0.1% vol. In each patient, 2 mL of the "Revixan" gel was administered to the mucous membrane of the posterior pharyngeal wall with a cotton swab. In 20 min after application the rest of the gel was removed, also with a cotton swab. After removal, a laser impact was performed at the wavelength of 405 nm with the light dose of 50 J/cm^2. The radiation was delivered to pharynx through a special diffusor emitting average irradiance of 0.2 W/cm^2 at a distance of 1.5 cm from the diffusor surface. The irradiation time was 250 s and the approximate area of the irradiated pharynx sector was 4×5 cm^2. Local anesthesia was not required for the PDT procedure. There were no patients with strong pharyngeal reflex enrolled in the study.

3 Results and Discussion

3.1 *Numerical Studies*

The simulated absorption maps for planar irradiation at the wavelength of 405 nm for skin and mucous tissues are shown in Figs. 1(a) and 1(b), respectively. The local absorbed

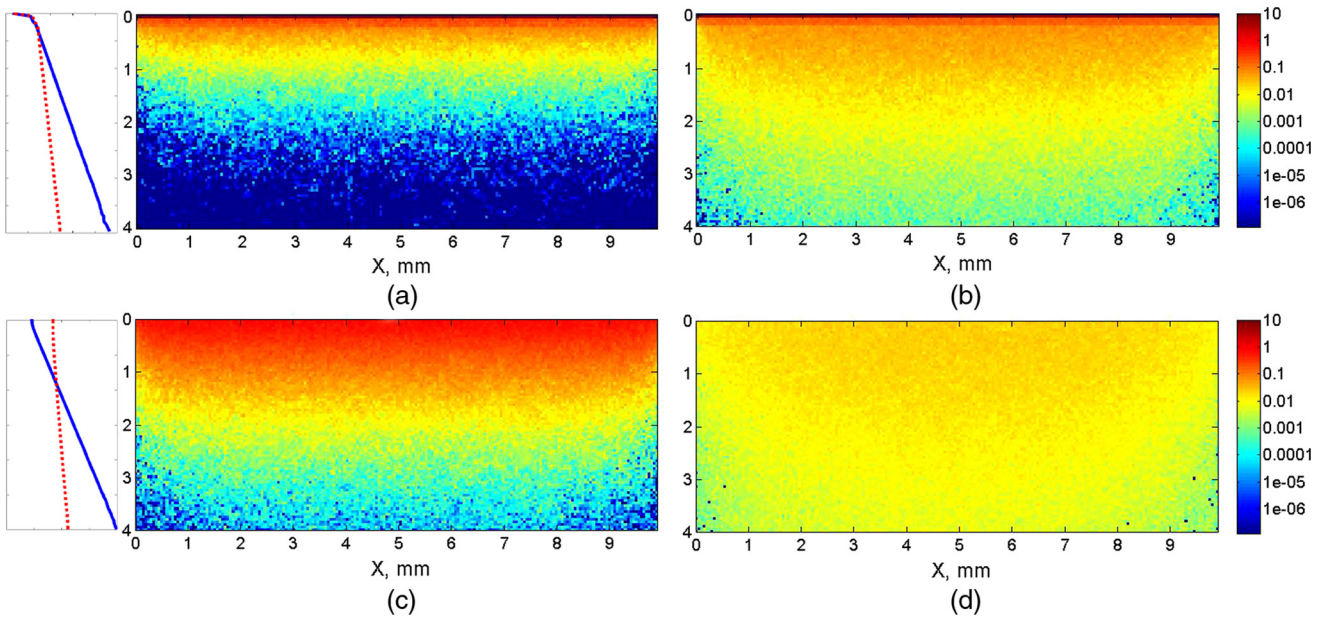

Fig. 1 Distribution maps of absorbed light dose density for (a, b) skin and (c, d) mucous tissue at a wavelength of (a, c) 405 nm and (b, d) 660 nm. Color encoding corresponds to the dose density in J/mm^3. The left panels demonstrate in-depth attenuation of local absorbed dose for 405 (blue line) and 660 (red line) nm.

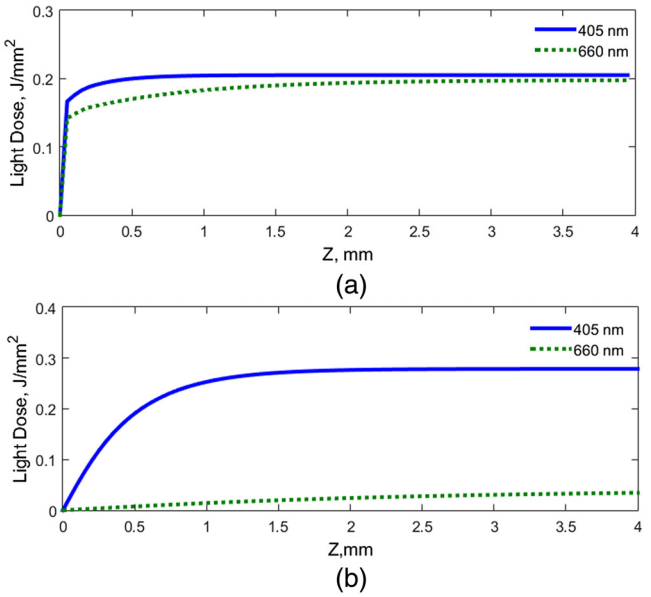

Fig. 2 Absorbed light dose at wavelengths of 405 and 660 nm in the tissue upper layer of thickness Z for (a) skin and (b) mucous tissue versus layer thickness.

dose densities are given in J per mm^3. Similar maps for the wavelength of 660 nm traditionally employed for PDT with chlorin-based PS are shown in Fig. 1(c) and 1(d) for comparison. The maps allow one to analyze the distribution of the absorbed dose over depth Z. For skin, the largest part of light energy is absorbed in the upper stratum corneum layer, whereas for mucosa the distribution is more uniform.

To quantitatively characterize the part of the total incident light intensity (0.5 J/mm^2) coming to the tissue surface, we built the dependence of the light intensity absorbed in the upper tissue layer on the layer thickness (Fig. 2). Unlike the absorption maps shown in Fig. 1, this dependence has a cumulative effect as it demonstrates the entire dose absorbed in the medium starting from the tissue surface down to the given depth Z, which is more critical in clinical applications where the dose delivered to the treated area should be evaluated. In the case of skin, the absorbed dose demonstrates a pronounced jump at small depths originating from the absorption in the stratum corneum layer; however, further increase in Z demonstrates slow growth because the major intensity was absorbed or backscattered in the upper layers. Surprisingly, for skin, the dependencies for the considered wavelengths do not differ dramatically. On the contrary, the single-layer model for mucous tissue demonstrates more steady increase of the absorbed dose with an increase in the layer thickness; however, the total absorbed dose varies greatly due to significant difference in the absorption coefficients of mucosa at 405 and 660 nm, respectively. All the demonstrated dependencies show saturation character indicating that lower depth contributes insignificantly to the total absorbed dose. For skin, for both wavelengths the saturation values lie around 0.20 J/mm^2 indicating that about 40% of the incident energy is absorbed within tissue, whereas the obtained dependencies demonstrate depth distribution. For mucosa, the saturation value for 405 nm is about 0.28 J/mm^2 indicating that around 56% of the incident intensity is absorbed. This value is higher than that for skin due to high scattering in stratum corneum resulting in high backscatter from the tissue. For 660 nm, the absorbed energy is much smaller approaching 0.03 J/mm^2 (6% of the incident intensity) for the layer thickness of 4 mm.

3.2 *Animal Studies*

In the animal study, accumulation of the PS within the tissue was confirmed by FI monitoring. Time evolution of the signals ratio at two excitation wavelengths indicated deeper penetration of PS into the tissue. The details of this approach to PDT monitoring are given in paper.[42]

Visual inspection revealed no changes in the skin of the rabbit ear after the PDT procedure in the course of 8-day monitoring.

Typical OCT-images of different parts of rabbit ear are shown in Figs. 3(a) and 3(d). The upper layer with a total thickness of approximately 300 μm with moderate signal corresponds to skin consisting of epidermis and dermis, superficial epidermis is thin and can hardly be resolved in the OCT image. The lower dark

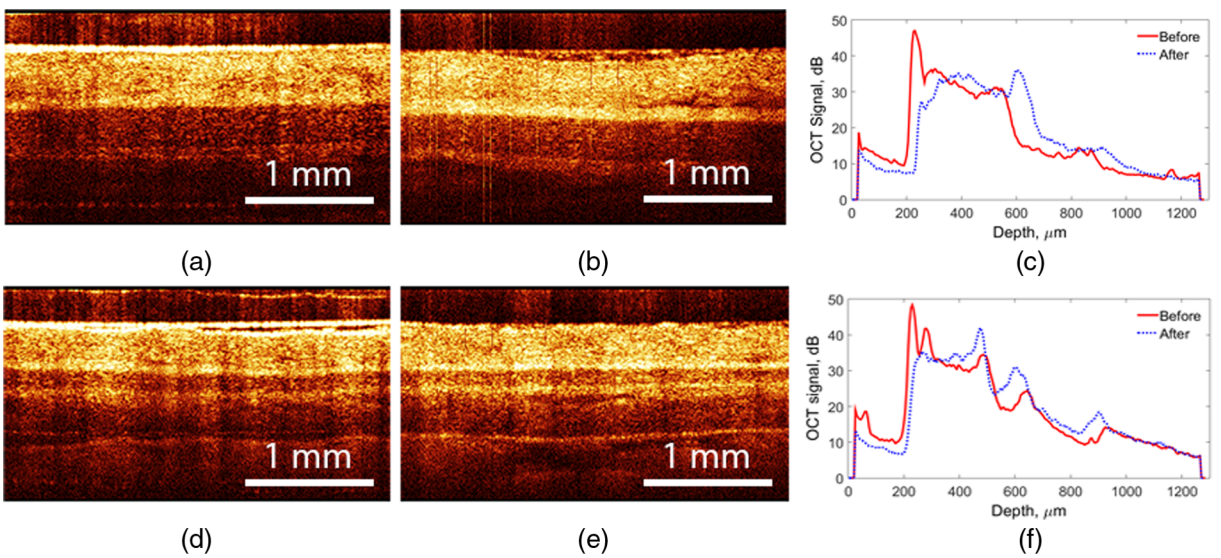

Fig. 3 OCT images of intact skin of rabbit ear (a, d) before and (b, e) after drug topical administration and (c, f) corresponding A-scans.

layer with thickness of about 150 μm corresponds to cartilage and is surrounded by two layers with high OCT signal corresponding to perichondrium (30- to 50-μm thick). Comparison of the intact tissue before and after drug application [Figs. 3(a) and 3(d) versus Figs. 3(b) and 3(e)] allows one to conclude that the drug acts as a clearing agent: it decreases scattering from the top tissue boundary and increases the signal from deeper layers. The gel, being the solvent of the PS, penetrates into the tissue resulting in refractive index matching, such as traditional clearing agents.[51] Especially pronounced is the increase in signals from the perichondrium and cartilage layers. To characterize this effect quantitatively, the A-scans before and after drug administration were plotted at the same graph [Figs. 3(c) and 3(f)]. Comparison of the one-dimensional in-depth OCT signal profiles (A-scans) confirms visually observed changes: the peak from the top boundary disappears, whereas the signals from perichondrium and cartilage rise. Clearing effect can serve as an indicator of drug penetration and, hence, PS accumulation in tissue and OCT can be employed to monitor PS penetration dynamics in case of topical application.

In the course of OCT monitoring, dark elongated areas with the low level of OCT signal were observed after the PDT procedure (Fig. 4); this effect was the most pronounced in 3 days after the procedure [Fig. 4(c)]. In 7 days after the first procedure, this manifestation became significantly weaker [Fig. 4(d)]. We associate this effect with appearance of edema in the area of treatment. This assumption is in agreement with the results of histological studies.

Angiography images allow one to monitor the response of the tissue microcirculatory system to the PDT procedure. Visual evaluation shows that in 3 days after the PDT procedure, smaller vessels become more pronounced in the angiographic OCT images and the vessel net becomes denser. Indirectly, this may serve as an indication of activation of small vessels.

Histological studies revealed that in 1 day after the PDT procedure, moderate edema is observed accompanied by moderate lymphohistiocytic infiltration with single neutrophils. The vessels have ordinary structure and their concentration corresponds to normal histology of a rabbit ear [Fig. 5(a)].

In 3 days after the PDT procedure, the histology inspection indicated the presence of a weak edema; however, the signs of inflammation were not detected. An increase in the area of newly formed vessel lumens in the histological images amounted 12% to 15%, which is associated with neoangiogenesis [Fig. 5(b)]. In 7 days after the PDT procedure, no edema or inflammation signs were revealed, whereas an increase in the area of the newly formed vessels reached 30% to 35% [Fig. 5(c)]. The results of the histological studies are summarized in Table 3.

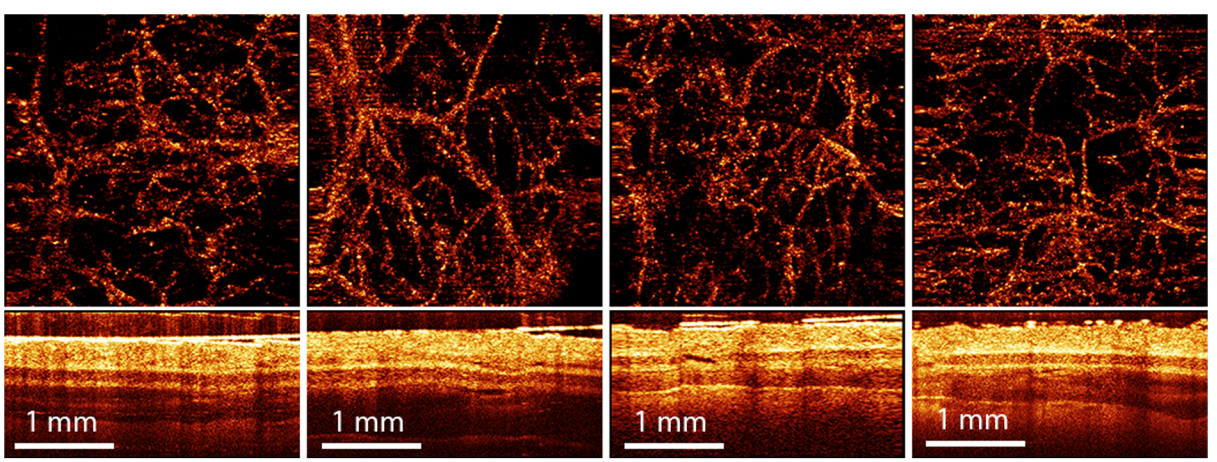

Fig. 4 (Top) Angiography and (bottom) structural OCT-images of (a) rabbit ear before, (b) in 1 day, (c) 3 days, and (d) 7 days after PDT procedure.

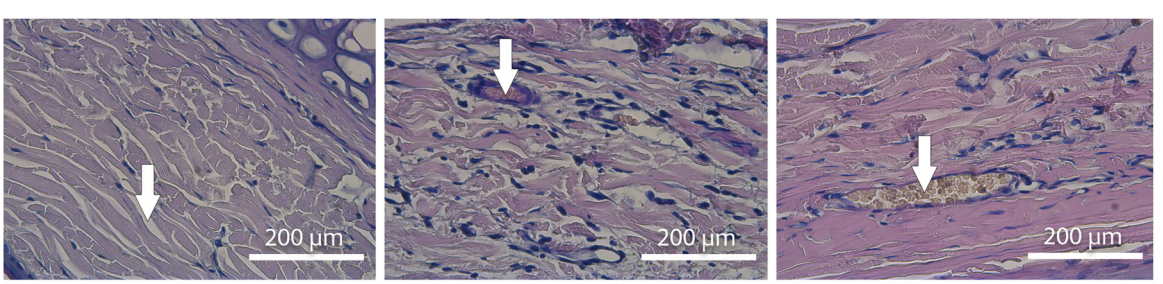

Fig. 5 Histology images (hematoxylin and eosin staining) of rabbit ear tissue in (a) 1, (b) 3, and (c) 7 days after PDT procedure. The arrows indicate (a) edema manifestation, (b) vessel with thick wall, and (c) newly formed vessel with thin wall.

Table 3 Manifestations in rabbit ear tissue after PDT procedure (histological studies).

	Edema	Inflammation	Average increase in the area of newly formed vessel lumens
In 1 day	++	+	5% ± 1.5%
In 3 days	+	–	13.5% ± 1.5%
In 7 days	–	–	32.5% ± 2.5%

3.3 *Clinical Studies*

OCT inspection of the posterior pharyngeal wall mucosa allowed one to distinguish two morphologically different cases: hyperthrophic and atrophic pharyngitis. In case of hypertrophic pharyngitis [Figs. 6(a) and 6(b)], the epithelial layer (upper layer with moderate signal in OCT image) is thickened and the boundary between epithelium and *lamina propria* (layer with high OCT signal) is not distinct. In subepithelial layer (lower layer in the OCT image), the elongated zones with low signal level are detected which is typical for edema. In case of atrophic pharyngitis [Figs. 6(c) and 6(d)], the epithelial layer is significantly thinned and can be hardly distinguished above *lamina propria*. The revealed differences in the OCT images allow one to preliminary conclude on the ability of OCT for differential diagnostics of chronic pharyngitis due to distinguishing specific morphologic features.

The criterion for inclusion a patient into the OCT-monitoring group was the exacerbation of pharynx chronic inflammatory disease with the indication for PDT treatment. Microbiological examination of the smears from the posterior pharyngeal wall mucosa preceded the PDT procedure indicating the presence of diverse microorganisms: *Staphylococcus haemolyticus*, *Staphylococcus aureus*, *Streptococcus pyogenes*, *Escherichia coli*, and other less common causative agents.

In the course of treatment, no complications or side effects of PDT were observed in the patients enrolled. The PDT procedure was well tolerated by all patients, no anesthesia was required; however, there were complaints of discomfort when applying PS to the posterior pharyngeal wall associated with different levels of pharyngeal reflex expression. After the PDT course, all the patients subjectively mentioned improved state of health.

Pharyngoscopy indicated the decrease of inflammatory processes (Fig. 7). In particular cases, hypervascularization of mucosa was visually noted [Fig. 7(c)]. Treatment efficiency was evaluated by patients' subjective feelings (complaints), pharyngoscopy inspection, and results of microbiological studies. Microbiological studies in all patients after the PDT course have not revealed any pathogenic flora; however, in particular cases activation of saprophytic flora was detected.

In six of eight patients positive changes were registered on the next day after the first PDT procedure (day 2), the patients noted stagnation of a discomfort in the throat, pharyngoscopy revealed local reaction manifested by hyperemia and contrasting of a vessel net. No progression of the local reactions was registered after the second and the third PDT procedures (days 2 and 3).

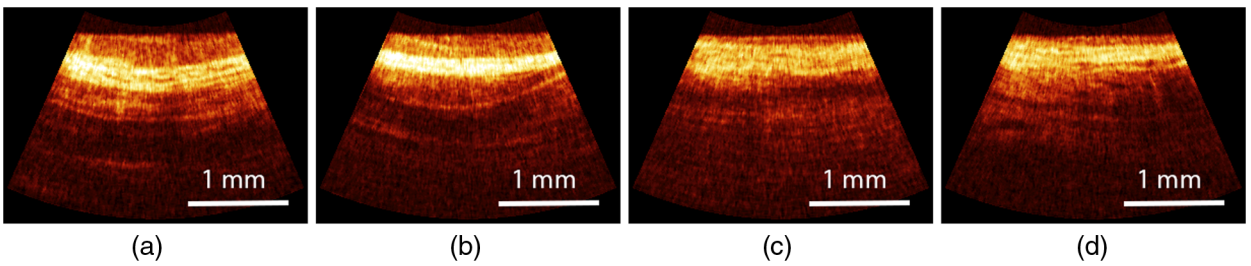

Fig. 6 Typical OCT-images of pharynx with (a, b) hypertrophic pharyngitis and (c, d) atrophic pharyngitis.

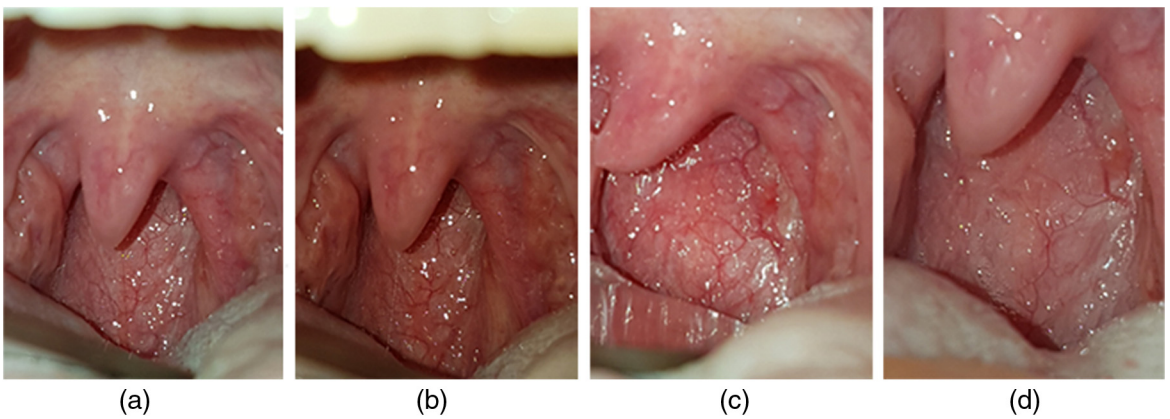

Fig. 7 Photographs of the posterior pharyngeal wall mucosa with chronic inflammatory process: (a) day 1, before PDT procedure (congestive hyperemia, edema of the palatine arch, expressed vascular pattern), (b) day 2 (increase of edema and hyperemia), (c) day 4 (hypervascularization, abatement of inflammatory manifestations), and (d) day 8 (abatement of inflammatory manifestations, decrease of hypervascularization).

In one patient with atrophic pharyngitis, improvement was registered only after the full PDT course (three procedures), the patient noted decrease of dryness in the throat and sensation of a foreign body, pharyngoscopy revealed increase in vascularization of the posterior pharyngeal wall mucosa and decrease in the amount of mucous secretion at the posterior pharyngeal wall. Another patient with long-term pathology (several years) did not note any dynamics in his state; although, pharyngoscopy indicated positive dynamics: decrease in chronic hyperemia and edema.

To reveal morphologic and functional alterations in the course of PDT, the OCT monitoring of the posterior pharyngeal wall mucosa was performed. Typical OCT images obtained in the course of PDT monitoring are shown in Fig. 8. Initially, the upper epithelial layer is thickened [Fig. 8(a)], the dark elongated zone in *lamina propria* corresponds to the lymphatic vessel, elongated zone under *lamina propria* corresponds to the blood vessel; longer zones of the low signal indicate the presence of edema. After application to the posterior pharyngeal wall mucosa, the solvent acts as a clearing agent [Fig. 8(b)]. An increase in the imaging depth and the signal level may serve as a criterion of PS penetration speed and depth. After PDT procedure [Fig. 8(c)] the response of the lymphatic system is observed, manifested by the increase in the number of the elongated dark areas. *Lamina propria* becomes inhomogeneous and disorganized with long areas of smaller signal associated with edema as a reaction to the procedure. On the day 2 more pronounced response to treatment is observed, confirmed by the visual inspection [Fig. 8(d)]. The second PDT procedure was performed on the day 2; after it, the response is observed at wider area, in addition, the edema remains pronounced in and under *lamina propria* [Fig. 8(e)]. In 1 day after the third PDT procedure (day 4), the edema becomes less manifested [Fig. 8(f)], *lamina propria* becomes denser. In 5 days after the third PDT procedure (day 8) *lamina propria* remains dense, the signs of edema disappear. A decrease in epithelium thickness indicates disappearance of infiltration. Comparison of the OCT-image obtained in 7 days after the start of the PDT course reveals better condition of the posterior pharyngeal wall mucosa with respect to its initial condition [Fig. 8(a)] indicating the efficiency of the performed treatment.

4 Conclusion

Development of the optimal protocols of PDT procedure is the key element in the success of PDT treatment. Presence of absorption peaks at 402 and 662 nm in chlorin-based PS[42] provides additional opportunities for the choice of irradiation regimens. Traditionally, the wavelengths around 660 nm are employed for irradiation due to deeper penetration in tissues; however, for superficial impact wavelengths around 405 nm could be beneficial, especially in case of antibacterial or antiaging PDT. In this paper, we analyzed different aspects of PDT performance at 405 nm: numerical simulations demonstrate absorbed dose distribution, animal and clinical experiments revealed tissue reaction to the PDT procedures. The study was performed for the light dose of 50 J/cm^2 usually employed for in antibacterial and cosmetic PDT.

OCT studies revealed that topical administration of the PS in the form of gel, which provides optical clearing in the OCT images; the effect was observed both in animal and clinical studies. Thus, OCT can be employed for evaluation of PS penetration into tissue prior to PDT procedure.

Further, both animal and clinical studies demonstrated that OCT can be efficiently employed for monitoring of tissue response to the procedure: activation of lymphatic system is manifested by an increase in the number of dark high-contrast inclusions in the OCT images, whereas edema is manifested by dark elongated areas. The absence of these manifestations in the course of OCT monitoring of PDT procedure could serve as an indication for correcting the PDT course.

Employment of OCT angiography in animal studies allowed one to visually detect changes in vessel net as a result of PDT procedure. Complementary histology studies revealed increase in the total area of blood vessel lumens after the PDT procedure

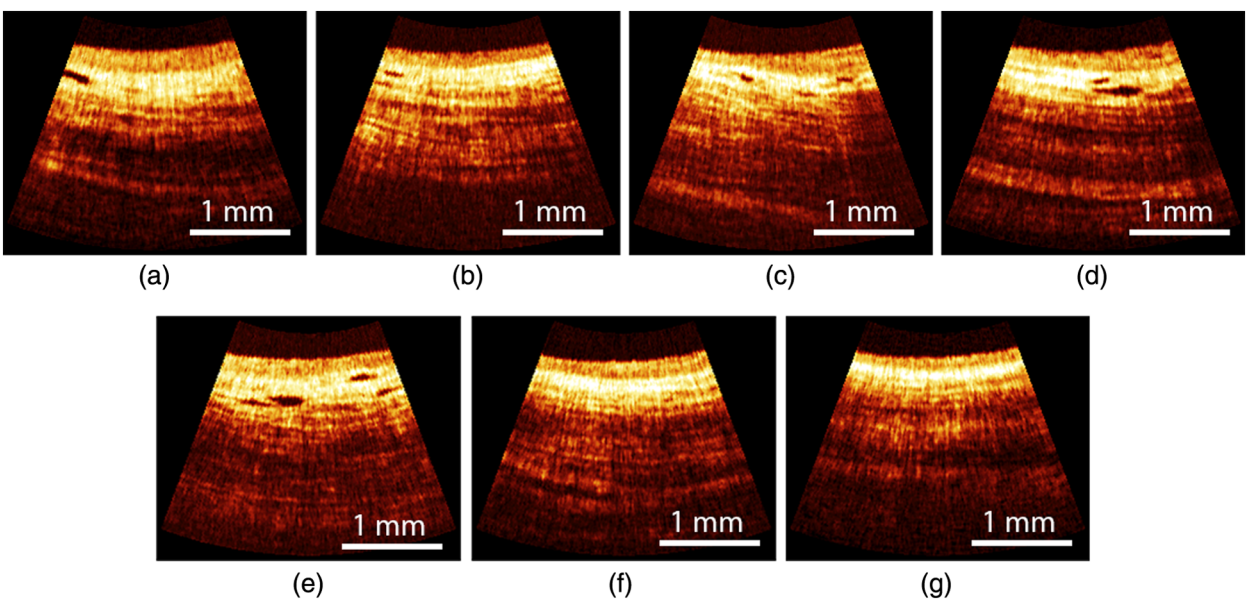

Fig. 8 OCT images of the posterior pharyngeal wall mucosa with exacerbation of chronic inflammation: (a) day 1, before PDT procedure, (b) day 1, after PS application, (c) day 1, immediately after PDT procedure, (d) day 2, before the PDT procedure, (e) day 2, after PDT procedure, (f) day 4, and (g) day 8.

allowing one to suppose PDT-induced neoangiogenesis that is in agreement with OCT angiography. However, for approval of this suggestion further immunohistochemical studies are required. Presumably, the effect of neoangiogenesis can be employed for correction of the atrophic alterations, in particular, chronic processes in ENT (ear, nose, and throat) organs, and stimulation of restorative processes in tissues. On the other hand, this effect is a contraindication for employment of the considered regime in anticancer PDT treatment.

Clinical studies revealed efficiency of the considered regimen in treatment of chronic pathologic processes of the ENT, whereas complementary OCT monitoring serves as a tool of personalized medicine allowing one to evaluate the PDT procedure outcome and, if necessary, correct the treatment tactics. Further studies require long-term monitoring of the outcomes of PDT treatment of pharynx atrophic pathologies.

Disclosures

The authors have no relevant financial interests in this article and no potential conflicts of interest to disclose.

Acknowledgments

The study was financed by Russian Science Foundation (RSF), Project #17-15-01264. The authors are thankful to Professor Natalia Shakhova for useful discussions, to Natalia Markina, and Valeria Perekatova for assistance in animal experiment. The authors acknowledge Revixan Ltd. (Russia) for provision of the drug.

References

1. P. Agostinis et al., "Photodynamic therapy of cancer: an update," *CA-Cancer J. Clin.* **61**(4), 250–281 (2011).
2. R. R. Allison and K. Moghissi, "Oncologic photodynamic therapy: clinical strategies that modulate mechanisms of action," *Photodiagn. Photodyn. Ther.* **10**(4), 331–341 (2013).
3. L. Huang, T. Dai, and M. R. Hamblin, "Antimicrobial photodynamic inactivation and photodynamic therapy for infections," *Methods Mol. Biol.* **635**, 155–173 (2010).
4. F. F. Sperandio, Y. Y. Huang, and M. R. Hamblin, "Antimicrobial photodynamic therapy to kill Gram-negative bacteria," *Recent Pat. Anti-Infect. Drug Discovery* **8**(2), 108–120 (2013).
5. X. Fu, Y. Fang, and M. Yao, "Antimicrobial photodynamic therapy for methicillin-resistant staphylococcus aureus infection," *BioMed. Res. Int.* **2013**, 159157 (2013).
6. L. M. Baltazar et al., "Antimicrobial photodynamic therapy: an effective alternative approach to control fungal infections," *Front. Microbiol.* **6**, 202 (2015).
7. M. Grinholc et al., "Antimicrobial photodynamic therapy with fulleropyrrolidine: photoinactivation mechanism of staphylococcus aureus, in vitro and in vivo studies," *Appl. Microbiol. Biotechnol.* **99**(9), 4031–4043 (2015).
8. E. T. Carrera et al., "The application of antimicrobial photodynamic therapy (aPDT) in dentistry: a critical review," *Laser Phys.* **26**(12), 123001 (2016).
9. J. S. Orringer et al., "Molecular effects of photodynamic therapy for photoaging," *Arch. Dermatol.* **144**(10), 1296–1302 (2008).
10. N. Bruscino et al., "Therapeutic hotline: facial skin rejuvenation in a patient treated with photodynamic therapy for actinic keratosis," *Dermatol. Ther.* **23**(1), 86–89 (2010).
11. R. Rossi, T. Lotti, and N. Bruscino, "Photodynamic therapy/assisted photorejuvenation," *J. Cosmet. Dermatol. Sci. Appl.* **1**(2), 30–35 (2011).
12. M. T. Wan and J. Y. Lin, "Current evidence and applications of photodynamic therapy in dermatology," *Clin. Cosmet. Invest. Dermatol.* **7**(3), 145–163 (2015).
13. A. Goldsberry and C. W. Hanke, "Photodynamic therapy for photoaging," *Curr. Dermatol. Rep.* **3**, 122–126 (2014).
14. M. Kim, H. Y. Jung, and H. J. Park, "Topical PDT in the treatment of benign skin diseases: principles and new applications," *Int. J. Mol. Sci.* **16**(10), 23259–23278 (2015).
15. J. P. Celli et al., "Imaging and photodynamic therapy: mechanisms, monitoring, and optimization," *Chem. Rev.* **110**(5), 2795–2838 (2010).
16. R. R. Allison and K. Moghissi, "Photodynamic therapy (PDT): PDT mechanisms," *Clin. Endosc.* **46**(1), 24–29 (2013).
17. J. C. Correa et al., "Previous illumination of a water soluble chlorine photosensitizer increases its cytotoxicity," *Laser Phys.* **22**(9), 1387–1394 (2012).
18. A. T. Dijkstra et al., "Photodynamic therapy with violet light and topical 6-aminolaevulinic acid in the treatment of actinic keratosis, Bowen's disease and basal cell carcinoma," *J. Eur. Acad. Dermatol. Venereol.* **15**(6), 550–554 (2001).
19. L.-W. Ma et al., "A new method for photodynamic therapy of melanotic melanoma—effects of depigmentation with violet light photodynamic therapy," *J. Environ. Pathol. Toxicol. Oncol.* **26**(3), 165–172 (2007).
20. S. Karrer et al., "Photodynamic therapy for skin rejuvenation: review and summary of the literature—results of a consensus conference of an expert group for aesthetic photodynamic therapy," *J. Dtsch. Dermatol. Ges.* **11**(2), 137–148 (2013).
21. M. D. Palm and M. P. Goldman, "Safety and efficacy comparison of blue versus red light sources for photodynamic therapy using methyl aminolevulinate in photodamaged skin," *J. Drugs Dermatol.* **10**, 53–60 (2011).
22. C. Thornfeldt, "Photodynamic therapy (PDT) utilizing multiple light sources significantly improves clinical efficacy and subject satisfaction with a review of PDT mechanisms of action," *Am. J. Cosmet. Surg.* **30**(2), 72–79 (2013).
23. M. Solomon et al., "Optical imaging in cancer research: basic principles, tumor detection, and therapeutic monitoring," *Med. Princ. Pract.* **20**(5), 397–415 (2011).
24. A. Taruttis and V. Ntziachristos, "Translational optical imaging," *Am. J. Roentgenol.* **199**(2), 263–271 (2012).
25. Y. Ardeshirpour et al., "Using in-vivo fluorescence imaging in personalized cancer diagnostics and therapy, an image and treat paradigm," *Technol. Cancer Res. Treat.* **10**(6), 549–560 (2011).
26. J. S. Tyrrell, S. M. Campbell, and A. Curnow, "The relationship between protoporphyrin IX photobleaching during real-time dermatological methyl-aminolevulinate photodynamic therapy (MAL-PDT) and subsequent clinical outcome," *Lasers Surg. Med.* **42**(7), 613–619 (2010).
27. T. M. Baran and T. H. Foster, "Fluence rate-dependent photobleaching of intratumorally administered pc 4 does not predict tumor growth delay," *Photochem. Photobiol.* **88**(5), 1273–1279 (2012).
28. M. Loshchenov et al., "Endoscopic fluorescence visualization of 5-ALA photosensitized central nervous system tumors in the neural tissue transparency spectral range," *Photonics Lasers Med.* **3**(2), 159–170 (2014).
29. S. Wang et al., "Light-controlled delivery of monoclonal antibodies for targeted photoinactivation of Ki-67," *Mol. Pharm.* **12**, 3272–3281 (2015).
30. S. C. Kanick et al., "Dual-channel red/blue fluorescence dosimetry with broadband reflectance spectroscopic correction measures protoporphyrin IX production during photodynamic therapy of actinic keratosis," *J. Biomed. Opt.* **19**, 075002 (2014).
31. N. R. Gemmell et al., "A compact fiber-optic probe-based singlet oxygen luminescence detection system," *J. Biophotonics* **10**(2), 320–326 (2017).
32. B. Li et al., "Photosensitized singlet oxygen generation and detection: recent advances and future perspectives in cancer photodynamic therapy," *J. Biophotonics* **9**(11–12), 1314–1325 (2016).
33. Z. Hamdoon et al., "Optical coherence tomography-guided photodynamic therapy for skin cancer: case study," *Photodiagn. Photodyn. Ther.* **8**(1), 49–52 (2011).
34. L. Themstrup et al., "Optical coherence tomography imaging of non-melanoma skin cancer undergoing photodynamic therapy reveals subclinical residual lesions," *Photodiagn. Photodyn. Ther.* **11**(1), 7–12 (2014).
35. M. A. Sirotkina et al., "Photodynamic therapy monitoring with optical coherence angiography," *Sci. Rep.* **7**, 41506 (2017).
36. U. Sunar et al., "Monitoring photobleaching and hemodynamic responses to HPPH-mediated photodynamic therapy of head and neck cancer: a case report," *Opt. Express* **18**, 14969–14978 (2010).
37. X. Yan et al., "Optical and photoacoustic dual-modality imaging guided synergistic photodynamic/photothermal therapies," *Nanoscale* **7**(6), 2520–2526 (2015).

38. S. Mallidi et al., "Prediction of tumor recurrence and therapy monitoring using ultrasound-guided photoacoustic imaging," *Theranostics* **5**(3), 289–301 (2015).
39. A. L. Maas et al., "Tumor vascular microenvironment determines responsiveness to photodynamic therapy," *Cancer Res.* **72**(8), 2079–2088 (2012).
40. M. Khurana et al., "Intravital high-resolution optical imaging of individual vessel response to photodynamic treatment," *J. Biomed. Opt.* **13**(4), 040502 (2008).
41. D. A. Loginova et al., "Probing depth in diffuse optical spectroscopy and structured illumination imaging: a Monte Carlo study," *J. Biomed. Photonics Eng.* **3**(1), 010303 (2017).
42. A. V. Khilov et al., "Two-wavelength fluorescence monitoring and planning of photodynamic therapy," *Sovrem. Tehnol. Med.* **9**(4), 96–105 (2017).
43. A. N. Bashkatov et al., "Optical properties of human skin, subcutaneous and mucous tissues in the wavelength range from 400 nm to 2000 nm," *J. Phys. D Appl. Phys.* **38**, 2543–2555 (2005).
44. E. Salomatina et al., "Optical properties of normal and cancerous human skin in the visible and near-infrared spectral range," *J. Biomed. Opt.* **11**(6), 064026 (2006).
45. V. V. Tuchin, *Tissue Optics: Light Scattering Methods and Instruments for Medical Diagnosis*, 3rd ed., SPIE Press, Bellingham, Washington (2015).
46. S. V. Patwardhan et al., "Monte Carlo simulation of light-tissue interaction: three-dimensional simulation for trans-illumination-based imaging of skin lesions," *IEEE Trans. Biomed. Eng.* **52**(7), 1227–1236 (2005).
47. C. H. Wilder-Smith et al., "Photoeradication of helicobacter pylori using 5-aminolevulinic acid: preliminary human studies," *Lasers Surg. Med.* **31**(1), 18–22 (2002).
48. S. Rajesh et al., "Antimicrobial photodynamic therapy: an overview," *J. Indian Soc. Periodontol.* **15**(4), 323–327 (2011).
49. M. R. Hamblin et al., "Photodynamic therapy: a new antimicrobial approach to infectious disease?" *Photochem. Photobiol. Sci.* **3**(5), 436–450 (2004).
50. M. S. Kleshnin et al., "Compact and fully automated system for monitoring photodynamic therapy, based on two LEDs and a single CCD," *Laser Phys. Lett.* **12**, 115602 (2015).
51. V. V. Tuchin, *Optical Clearing of Tissues and Blood*, SPIE Press, Bellingham, Washington (2005).

Maria Shakhova is an assistant of the Department of ENT Diseases of Privolzhskiy Research Medical University and an otorhinolaryngologist at N.A. Semashko Nizhny Novgorod Regional Hospital. She graduated from Nizhny Novgorod State Medical Academy in 2003. Her scientific interests include laser surgery, optical bioimaging, and photodynamic therapy. She has coauthored publications in peer-reviewed journals and conference proceedings.

Daria Loginova is a second-year master's student at the Lobachevsky State University of Nizhny Novgorod and a junior researcher at the Laboratory of Biophotonics at the Institute of Applied Physics of the Russian Academy of Sciences. Her scientific interests include Monte Carlo numerical simulations of light transport in biotissues in the application to bioimaging modalities (optical diffuse reflectometry, OCT) and photodynamic therapy.

Alina Meller is an assistant at the Department of ENT Diseases of Privolzhskiy Research Medical University and an otorhinolaryngologist at N.A. Semashko Nizhny Novgorod Regional Hospital. She graduated from Nizhny Novgorod State Medical Academy in 2011. Her scientific interests include biophotonics, optical bioimaging, and photodynamic therapy. She has coauthored publications in peer-reviewed journals and conference proceedings.

Dmitry Sapunov is an assistant of the Department of ENT Diseases of Privolzhskiy Research Medical University and an otorhinolaryngologist at N.A. Semashko Nizhny Novgorod Regional Hospital. He graduated from Nizhny Novgorod State Medical Academy in 2010. His scientific interests include biophotonics, optical bioimaging, and photodynamic therapy. He has coauthored publications in peer-reviewed journals and conference proceedings.

Natalia Orlinskaya is the head of the Pathologic Anatomy Division of the Privolzhskiy Research Medical University and a professor with the Chair of Pathologic Anatomy. She graduated from Nizhny Novgorod State Medical Academy in 1996. Her scientific interests include experimental medicine, pathomorphology of the thyroid gland, the gastrointestinal tract, and human tumors. She has coauthored more than 80 papers and a monograph.

Andrey Shakhov is the head of the ENT Diseases Chair of the Privolzhskiy Research Medical University. He graduated from S.M. Kirov Gorky Medical Institute in 1978 and received his DSc degree in the area of clinical applications of optical coherence tomography. His scientific interests include ear microsurgery, radio diagnostics, and functional surgery of throat pathologies, nose endosurgery. He has coauthored more than 50 papers and 3 monographs.

Alexander Khilov is a PhD student at the Institute of Applied Physics of Russian Academy of Sciences. He received his master's degree from Nizhny Novgorod State University (Russian Federation) in 2013. His scientific interests include fluorescent imaging, optical coherence tomography, and photodynamic therapy. He has coauthored publications in peer-reviewed journals and conference proceedings.

Mikhail Kirillin is a senior researcher at the Laboratory of Biophotonics at the Institute of Applied Physics of the Russian Academy of Sciences. He received his PhD from Moscow State University, Russia, in 2006 and his DSc (Tech) degree from the University of Oulu, Finland, in 2008. His scientific interests include biomedical imaging modalities, theoretical description, and numerical simulations of light transport in biotissues and other scattering media (in particular, Monte Carlo technique), and photodynamic therapy.